On the Perturb-and-Observe and Incremental Conductance MPPT Methods for PV Systems

Article *in* IEEE Journal of Photovoltaics · July 2013

DOI: 10.1109/Jphotov.2013.2261118

5 authors, including:

Dezso Sera
Aalborg University
107 PUBLICATIONS **2,599** CITATIONS
SEE PROFILE

Laszlo Mathe
Aalborg University
51 PUBLICATIONS **585** CITATIONS
SEE PROFILE

Tamás Kerekes
Aalborg University
99 PUBLICATIONS **3,032** CITATIONS
SEE PROFILE

Sergiu Viorel Spataru
Aalborg University
45 PUBLICATIONS **501** CITATIONS
SEE PROFILE

On the Perturb-and-Observe and Incremental Conductance MPPT methods for PV systems

Dezso Sera, *Member, IEEE*, Laszlo Mathe, *Member, IEEE*, Tamas Kerekes, *Member, IEEE*, Sergiu Spataru, *Student Member, IEEE*, Remus Teodorescu, *Fellow, IEEE*

***Abstract*— This paper presents a detailed analysis of the two most well-known hill-climbing MPPT algorithms, the Perturb-and-Observe (*P&O*) and Incremental Conductance (*INC*). The purpose of the analysis is to clarify some common misconceptions in the literature regarding these two trackers, therefore helping the selection process for a suitable MPPT for both researchers and industry. The two methods are thoroughly analyzed both from mathematical and practical implementation point of view. Their mathematical analysis reveals that there is no difference between the two. This has been confirmed by experimental tests according to the EN 50530 standard, resulting in a deviation between their efficiencies of 0.13% in dynamic, and as low as 0.02% in static conditions.**

The results show that despite the common opinion in the literature, the *P&O* and *INC* are equivalent.

***Index Terms*— MPPT, Perturb and Observe, Incremental Conductance, Discrete implementation, Photovoltaic systems**

I. Introduction

Maximum Power Point Tracking (MPPT) is one of the key functions that every grid-connected PV inverter should have. There is a large amount of publications dealing with MPPT, and trackers in the majority of the commercial PV inverters are able to extract around 99% of the available power from the PV plant, over a wide irradiance and temperature range - at least in steady state [1]. An extensive overview of modern MPPT techniques has been presented in [2].

The two most frequently discussed MPPT algorithms are the *P&O* and the *INC*. These methods are based on the fact that, on the voltage-power characteristic, the variation of the power w.r.t. voltage is positive ($dP/dV > 0$) in the left-hand side of the Maximum Power Point (MPP), while it is negative ($dP/dV < 0$) on the right-hand side of MPP.

The main advantages of these methods are that they are generic, e.g. suitable for any PV array, they do not require any information about the PV array, they work reasonably well in most conditions, and they are simple to implement on a digital controller.

A detailed literature review today would lead to the conclusion that although the *INC* is slightly more complicated to implement, it provides better performance than *P&O* in both static and dynamic conditions. The two main problems of the *P&O* frequently mentioned in the literature, are the oscillations around the MPP in steady state conditions, and the poor tracking (possibly in the wrong direction, away from MPP) under changing irradiance [3]–[14]. Methods to improve the dynamic behavior of the *P&O*, including variable step size and perturbation frequency have been reported in the literature [4], [5], [8], [15]–[18].

On the other hand, it is often stated in the literature that the *INC* can determine the position of the actual operating point relative to the MPP, and it can find the distance to it; it can also stop perturbing when the MPP has been reached, thus offering a superior performance to the *P&O*. It is also often stated that *INC* can track fast changing irradiance better than *P&O,* e.g. [2], [5], [12], [14], [17], [19]–[30].

Typical statements include "The [*INC*] method […] has been proposed to improve the tracking accuracy and dynamic performance under rapidly varying conditions" [7], "The disadvantage of the *P&O* method can be improved by comparing the instantaneous panel conductance with the incremental panel conductance" [11], "[*INC*] gives a good performance under rapidly changing conditions"[11], "Incremental conductance can determine that the MPPT has reached the MPP and stop perturbing the operating point", "[*INC*] can track rapidly increasing and decreasing irradiance conditions with higher accuracy than *P&O"*[10].

In a recent work [31], both the *P&O* and *INC* have been implemented on a commercial PV inverter, challenging the common belief of higher *INC* performance. The performance of these two methods using various perturbation amplitudes and frequencies has been compared. The results "suggest that the two algorithms are similar"[31]; however, the author does not provide mathematical explanation of why the two methods perform so similarly.

The aim of this work is to provide theoretical and experimental proof that *P&O* and *INC* are equivalent, and to clarify some of the common misconceptions in the literature regarding these two trackers. Furthermore, this paper provides a thorough analysis of these two that can help the industry and researchers in choosing the right tracker for a given application. In Section II it is mathematically proven that the *P&O* and *INC* are equivalent both in static and dynamic conditions, and in Section III this is confirmed by experimental tests according to the EN 50530 [32] standard.

II. *Analysis of P&O* and *INC*

A. Operating principle of P&O and INC

The *P&O* is probably the most often used MPPT algorithm today, due to its simplicity and generic nature [33]–[35].

It is based on the fact that on the derivative of power in

D. Sera, L. Mathe, T. Kerekes, S. Spataru and R. Teodorescu are with the Department of Energy Technology, Aalborg University, Aalborg, DK-9220, Denmark (e-mail: des@et.aau.dk, lam@et.aau.dk, tak@et.aau.dk; ssp@et.aau.dk, ret@et.aau.dk)

function of voltage is zero at MPP. At an operating point on the P-V curve, if the operating voltage of the PV array is perturbed in a given direction and $dP > 0$, it is known that the perturbation moved the array's operating point towards the MPP. The *P&O* algorithm would then continue to perturb the PV array voltage in the same direction. If $dP < 0$, then the change in operating point moved the PV array away from the MPP, and the *P&O* algorithm reverses the direction of the perturbation. In this paper the nonlinear characteristic of the PV array is reproduced using the single-diode 5-parameter model, in accordance with the requirements of the EN 50530. A detailed description of this model can be found in [36].

The second well-known MPPT algorithm, the *INC* [37] claims to improve the *P&O* by replacing the derivative of the power versus voltage *dP/dV* used by the *P&O* with comparing the PV array instantaneous (*I/V*) and incremental (*dI/dV*) conductance. These terms are obtained by manipulating the *dP/dV* equation, as shown in equations (1) and (2).

The derivative of power in function of voltage at MPP can be expressed in mathematical form as:

$$\left.\frac{\partial P}{\partial V}\right|_{\substack{P=P_{mp}\\V=V_{mp}}} = 0 \tag{1}$$

Rewriting (1) by replacing *P* with *VI*, results in (2):

$$\left.\frac{\partial (VI)}{\partial V}\right|_{\substack{I=I_{mp}\\V=V_{mp}}} = 0 \Rightarrow V_{mp}\left.\frac{\partial I}{\partial V}\right|_{\substack{I=I_{mp}\\V=V_{mp}}} + I_{mp} = 0 \tag{2}$$

In the above equations, V_{mp} is the voltage at MPP, and I_{mp} is the current at MPP.

The first incremental conductance – based algorithm was proposed in [38], where an analogue implementation was presented. In [38], the term *dI/dV* has been calculated based on a harmonic component in the PV array voltage and current, which is independent from the perturbation of the MPPT, and is not affected by changing irradiance.

However, the discrete implementation that became the well-known *INC* algorithm proposed in [37], has an essential difference from the analogue implementation proposed in [38]. In [37], *dI/dV* is identified based on the tracker's own perturbations; therefore it is not immune to the changing irradiance.

B. Mathematical comparison in continuous time

From equations (1) and (2) can be seen that dividing equation (2) by V_{mp} will not change its value at *MPP* (since $\delta P/\delta V$ is zero at MPP). However, it has a scaling effect everywhere else on the *IV* curve.

Considering an arbitrary point on the *IV* curve, one can write the mathematical expression based on which the *P&O* decides the next perturbation direction:

$$\delta_{PO} = \partial P/\partial V \tag{3}$$

While *P&O* decides the direction of the next perturbation based on the sign of δ_{PO}, *INC* decides based on δ_{INC}, as shown below:

$$\delta_{INC} = \partial I/\partial V + I/V \tag{4}$$

From (2), (3), and (4), it is obvious that:

$$\delta_{INC} = \delta_{PO}/V \tag{5}$$

From mathematical point of view (in continuous time), this factor of *I/V* is the only difference between the two methods, which - considering that the PV array voltage is always positive - will not change the sign of δ_{INC} compared to δ_{PO} at any point on the *IV* curve. Therefore, two trackers that base their tracking on $\delta_{PO,}$ and δ_{INC} respectively will have perfectly identical behavior.

C. Discrete implementation of P&O and INC

In practice, both *P&O* and *INC* are implemented in discrete time, with various update frequencies, usually between 1-20Hz [31], [39], [40].

The discrete form of equation (3) becomes:

$$\nabla_{PO} = \frac{P_k - P_{k-1}}{V_k - V_{k-1}} = \frac{\Delta P}{\Delta V} \tag{6}$$

Where ∇_{PO} is the discrete form of $\delta_{PO,}$ $P_k = I_k V_k$, and $P_{k-1} = I_{k-1}V_{k-1}$. The other notations have the following meaning: P_k, V_k, I_k – the power, voltage, and current at the *k*-th (actual) sampling instance; $P_{k-1}, I_{k-1}, V_{k-1}$ – the power, voltage, and current at the previous sampling instance.

Looking at the case of *INC*, the discrete implementation of (4) usually takes the form below:

$$\nabla_{INC} = \frac{I_k - I_{k-1}}{V_k - V_{k-1}} + \frac{I_k}{V_k} = \frac{\Delta I}{\Delta V} + \frac{I_k}{V_k} \tag{7}$$

Where ∇_{INC} is the discrete version of δ_{INC}. Other discrete implementations of (4) can be done by using forward or central differences. In this paper, the discrete implementation according to [37], which is shown in eq.(7), will be analyzed.

In order to compare the *P&O* and *INC* in discrete, the differences between eq. (6) and (7) are calculated, analogously to (5), defined as:

$$\varepsilon = \nabla_{INC} - \nabla_{PO}/V_k \tag{8}$$

From the above, ε can be calculated as:

$$\varepsilon = \Delta I/V_k \Leftrightarrow \varepsilon \neq 0\big|_{\Delta I \neq 0} \tag{9}$$

Eq. (9) shows that the equality in (5) is no longer fulfilled in discrete. This difference is due to the fact that the discrete implementation of *INC* ignores the last term in the backward difference of *P,* which can be expressed as:

$$\Delta P = \Delta(I \cdot V) = \Delta I \cdot V_k + \Delta V \cdot I_k - \Delta I \cdot \Delta V \tag{10}$$

As a result, the discrete counterpart of (5) becomes:

$$\nabla_{INC} = \frac{\nabla_{PO}}{V_k} + \frac{\Delta I}{V_k} = \frac{\nabla_{PO}}{V_k} + \varepsilon \tag{11}$$

The extra checks (*ΔV=0?*, *ΔI =0?,*) performed by the *INC* will not be analyzed here, since in one hand they can be equally applied to both the *P&O* and *INC*, and on the other hand these conditions are met extremely rarely in a practical application [37]. In the following, the effects of the discretization error will be investigated.

D. Effects of the discretization error in static conditions

Equation (9) shows that the discrete implementation of *INC* introduces an error in addition to the *P&O*. This means that theoretically a situation can exist, where the sign of ∇_{INC} is different from the sign of ∇_{PO} , leading to a different direction of the next perturbation. It can be easily seen that the relative

size of the error (ε) compared to ∇_{INC} is maximum in the vicinity of the MPP, where both ∇_{INC} and ∇_{PO} tend to zero.

It will be shown below that as long as V_k and V_{k-1} are on the same side of the MPP (the last perturbation did not move the operating point from one side of the MPP to the other), the error (ε) will not affect the next perturbation direction. (The situation where the perturbation moves the operating point from one side to the other of the MPP will be discussed in the next subsection II.D.2).

1) $V_k > V_{mp}$ and $V_{k-1} > V_{mp}$, or $V_k < V_{mp}$ and $V_{k-1} < V_{mp}$

In order to evaluate the effect of ε on the tracking of *INC*, first an 'ideal' ∇^*_{INC} is defined, which assumes that (5) is valid also in discrete:

$$\nabla^*_{INC} = \nabla_{PO}/V_k \Rightarrow \nabla^*_{INC} = \nabla_{INC} - \varepsilon \tag{12}$$

Secondly, the worst case scenario – where the relative size of ε compared to ∇^*_{INC} is the maximum – should be determined. On a given *IV* curve, the relative size of ε is the maximum at the MPP, since ∇^*_{INC} tends to zero at this point. A worst case scenario for a given *IV* curve can then be considered:

$$\begin{cases} V_{k-1} = V_{mp} \pm \Delta V \\ V_k = V_{mp} \end{cases}, or \begin{cases} V_{k-1} = V_{mp} \\ V_k = V_{mp} \pm \Delta V \end{cases} \tag{13}$$

However, *IV* curves with different Fill Factors (FF = $I_{sc}V_{oc}/(I_{mp}V_{mp})$) can produce different values of ∇_{PO} (and ∇^*_{INC}) in the vicinity of MPP. Fig. 1 shows that as FF decreases, the power-voltage (*P-V*) curve becomes flatter, and in the same time ∇_{PO} and ∇^*_{INC} decreases in the vicinity of MPP. The flattest *P-V* curve corresponds to the case when the *IV* curve becomes a straight line from I_{sc} to V_{oc}.

It can be seen from Fig. 1 that by taking a finite ΔV at the MPP (according to (13)), ∇_{PO} has the lowest value for the case of *FF*=0.25. In the same time, the smallest *FF* also produces the largest error ε at the MPP, as shown in Fig. 2.

Therefore, the straight *IV* curve with *FF* = 0.25 will be considered as the worst case scenario to show that while V_k and V_{k-1} are on the same side of the MPP, the error ε is smaller than ∇^*_{INC}.

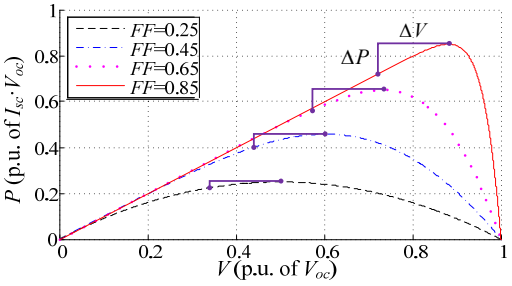

Fig. 1: *P-V* curves at various *FF*s. The case of *FF*=0.25 results in a straight line from I_{sc} to V_{oc} on the *IV* curve

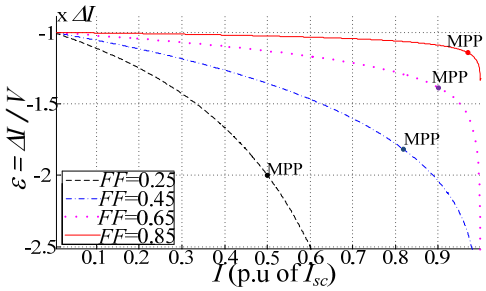

Fig. 2: Relative values of the error $\varepsilon = \Delta I/V$ for *IV* curves with different *FF*s. The largest absolute value for ε at MPP is obtained by the curve with *FF* = 0.25.

Being *IV* a straight line from I_{sc} to V_{oc}, the equation of the *IV* curve becomes:

$$I = I_{sc} - V I_{sc}/V_{oc} \tag{14}$$

While the power can be expressed as:

$$P = I \cdot V = -V^2 I_{sc}/V_{oc} + V I_{sc} \tag{15}$$

For this case, the derivative of the power w.r.t. voltage is:

$$\partial P/\partial V = \delta_{PO} = -2V I_{sc}/V_{oc} + I_{sc} \tag{16}$$

In discrete, at a distance of $\pm\Delta V$ from V_{mp}, the above equation can be written as:

$$\nabla_{PO}\big|_{V_{mp}\pm\Delta V} = -2\left(V_{mp} \pm \Delta V\right)\frac{I_{sc}}{V_{oc}} + I_{sc} \tag{17}$$

Considering the operating point at a distance of $\pm\Delta V$ from MPP as shown in Fig. 1, (the 2nd order *P-V* curve is symmetric w.r.t V_{mp}), the expression of ε from (8) can be written for the present case as:

$$\varepsilon\big|_{V_{mp}\pm\Delta V} = \frac{\Delta I}{V_{mp} \pm \Delta V} \tag{18}$$

Inserting equation (17) into (12), and considering that for a straight *IV* curve (see eq.(14)) $V_{mp}=V_{oc}/2$, and $I_{mp}=I_{sc}/2$, the ratio of error ε and ∇^*_{INC} can be determined, resulting in (19):

$$\frac{\varepsilon\big|_{V_{mp}\pm\Delta V}}{\nabla^*_{INC}\big|_{V_{mp}\pm\Delta V}} = \frac{1}{2} \tag{19}$$

In other words, at the operating point of $V_{mp} \pm \Delta V$ in a 2nd order *PV* curve, $\nabla_{INC} = \nabla^*_{INC} \pm \nabla^*_{INC}/2$. This also means that ε is not able to change the sign of ∇^*_{INC} thus cannot alter the tracking decision of *INC* compared to *P&O*.

To conclude the above, it can be said that in *static conditions*, as long as the operating point does not cross the MPP during the perturbation period, the error due to discretization cannot exceed 50% for the considered worst case scenario of *FF*=0.25.

2) $V_{k-1} < V_{mp} < V_k$ or $V_{k-1} > V_{mp} > V_k$

According to (11), a situation can theoretically exist when the perturbation direction of the *INC* can be altered compared to *P&O*. However, as shown before, this can only happen in the event when the perturbation moves the operating point *across* the MPP (see Fig. 3 below) such that $|\Delta P| < |\Delta I \cdot \Delta V|$.

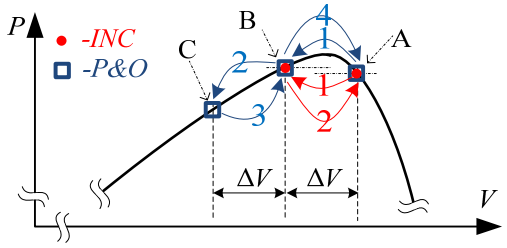

Fig. 3: Movement of the operating point around the MPP for *P&O* and *INC*, for the case when $|\varepsilon| > |\nabla^*_{INC}|$.

The above figure shows an interesting consequence of the imperfect discrete differentiation on which the *INC* is based (see equations (10) and (11)). A situation can exist, where the *INC* is 'stuck' to the MPP, and stays within one perturbation distance ΔV from V_{mp}. That is due to the fact that the sign of ∇_{INC} is determined by the sign of ΔI, which forces the *INC* to change direction at each perturbation and hence oscillate between A and B. However, this is not related to its credited capability that it can determine when the MPPT has reached the MPP [10], [37] it is merely a consequence of the discrete differentiation error and can only occur in specific circumstances.

It is worth noting that the effect of ε on the tracking of *INC* is masked in practical cases, when measurement error, noise and ripple are present, as shown by the experimental tests.

E. Dynamic behavior of P&O and INC

Fig. 4 shows the situation when an increase in irradiance occurs during the MPPT update period. If the MPPT takes a sample of the measured power at the instance (*k-1)*, i.e. P_{k-1}, then takes the next sample at the sampling instance *k*, the calculated $\Delta P = P_k - P_{k-1}$ will contain the power change due to the perturbation (ΔP^{PO}), but also the change due to the increased irradiance (ΔP^{G}).

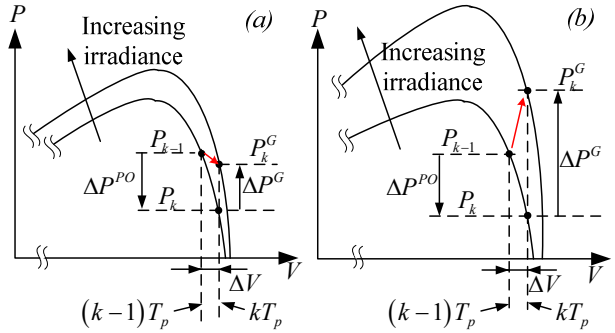

Fig. 4: Effect of the irradiance change during a perturbation period for the *P&O*. In case of slow irradiance changes, *P&O* is able to determine the right tracking direction (*a*), while a fast changing irradiance can cause it to track in the wrong direction (*b*). [41]

In the above figure, the notations have the following meaning: T_p – the sampling period of the MPPT; P_k^G – the power value at the *k*-th sampling instance when irradiance change occurred; $\Delta P^{PO} = P_k - P_{k-1}$– the change in power caused by the MPPT action alone; $\Delta P^G = P_k^G - P_{k-1}$– the change in power caused by the increase in irradiation alone; ΔV– the voltage increment of the MPPT.

The overall change of power during the MPPT sampling period can be expressed as:

$$\Delta P = P_k^G - P_{k-1} = \Delta P^{PO} + \Delta P^G \quad (20)$$

Therefore, in case of opposite signs for ΔP^{PO} and ΔP^G the sign of ΔP will be determined by the larger one.

In case of *INC*, the above situation is illustrated in Fig. 5:

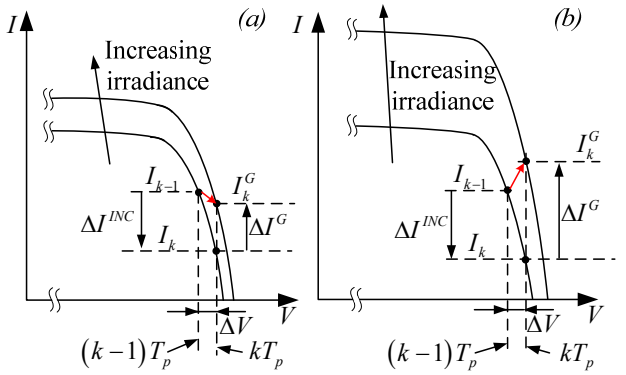

Fig. 5: Illustration of the effect of irradiance change during a perturbation period for the *INC*. Equally to the *P&O*, fast changing irradiance can cause the *INC* to track in wrong direction.

In the above figure, the notations have the following meaning: I_{k-1}, I_k^G – the current values measured at the *k-1*-th and the *k*-th sampling instances; I_k– the current at sampling instance *k* when no change in irradiance occurred; $\Delta I^{INC} = I_k - I_{k-1}$– the change in current caused by the perturbation of the MPPT; $\Delta I^G = I_k^G - I_k$– the change in current caused by the increased irradiation.

Similarly to the case of *P&O*, if ΔI^{INC} and ΔI^G have different signs, the sign of ΔI will be determined by the larger one (see Fig. 5):

$$\Delta I = I_k^G - I_{k-1} = \Delta I^{INC} + \Delta I^G \quad (21)$$

1) Boundary conditions of correct tracking for P&O

For both the *P&O* and *INC* in changing irradiance, one can write the boundary conditions for correct tracking. In case of the *P&O*, this is met when the amplitude of ΔP^G becomes larger and with opposite direction compared to ΔP^{PO}.

In order to compare the behavior of the *P&O* and *INC* in changing conditions, a reference irradiance ramp is considered, for which, at a given point on the *IV* curve, the following condition for the *P&O* is fulfilled:

$$\nabla_{PO} = 0 \Leftrightarrow \Delta P = 0 \Leftrightarrow \Delta P^{PO} = -\Delta P^G \quad (22)$$

where ΔP is the total change of power within an MPPT sampling period, according to (20). This is the limit condition for which the *P&O* can decide the correct tracking direction. The condition in (22) can be written as:

$$P_k^G = P_{k-1} \Leftrightarrow I_k^G V_k = I_{k-1} V_{k-1} \Rightarrow I_k^G = I_{k-1} V_{k-1} / V_k \quad (23)$$

In the following, it is verified whether for the same irradiance ramp, at the same point on the *IV* curve, the *INC* is able to track in the correct direction, or gets confused.

2) Boundary conditions for correct tracking for INC

Considering the same conditions as in (22), ∇_{INC} will take the form:

$$\nabla_{INC} = \frac{I_k^G - I_{k-1}}{V_k - V_{k-1}} + \frac{I_k^G}{V_k} \tag{24}$$

After bringing the two fractions in (24) to the same denominator, and replacing I_k^G with its expression from (23), will result in ∇_{INC} as follows:

$$\nabla_{INC} = -\frac{I_{k-1}(V_k - V_{k-1})}{V_k^2} = -\frac{I_{k-1}}{V_k^2}\Delta V \tag{25}$$

It can be seen from the above that, as long as $\Delta V \neq 0$, ∇_{INC} is also non-zero. Therefore, in the conditions described by (22) the *INC* may not behave identically to the *P&O*. In order to assess the effect of this difference on the tracking of the *INC* in changing conditions, the four main cases that can bring the *P&O* to the limit condition in (22), are considered. The sign of ∇_{INC} in these situations will indicate whether the *INC* gets confused or not in the limit conditions of *P&O*.

a) $V_{mp,k-1} < V_{k-1} < V_k$, *Increasing irradiance*

This corresponds to the situation when the operating point is on the right-hand side of the MPP voltage (V_{mp}), and the last perturbation moved the operating point away from the MPP, while the irradiance increased. In this case, while $\nabla_{PO} = 0$, (25) will result in $\nabla_{INC} < 0$, which means that *INC* is able to take the *correct decision* for the next perturbation.

b) $V_{mp,k-1} < V_k < V_{k-1}$, *Decreasing irradiance*

In this second case, the operating point is also on the right-hand side of the MPP, but now the last perturbation moved the operating point towards the MPP, and the MPPT can be potentially confused by the decreasing irradiation. In this situation, while $\nabla_{PO} = 0$, (25) will result in $\nabla_{INC} > 0$ Being on the right-hand side of the MPP, this implies a *wrong decision* regarding the next perturbation's direction.

c) $V_k < V_{k-1} < V_{mp,k-1}$, *Increasing irradiance*

The third case shows the situation where the operating point is on the left-hand side of the MPP, the last perturbation moved the operating point away from the MPP, and the MPPT can get confused due to the increasing irradiation. In this case, while $\nabla_{PO} = 0$, (25) will result in $\nabla_{INC} > 0$ since $V_k < V_{k-1}$. Being on the left-hand side of the MPP, this means a *correct decision* for the next perturbation.

d) $V_{k-1} < V_k < V_{mp,k-1}$, *Decreasing irradiance*

The last case considers the situation, where on the left-hand side of the MPP, the tracker just moved the operating point towards the MPP, but it potentially gets confused due to the decreasing irradiation that occurs in the same time. In this case, while $\nabla_{PO} = 0$, (25) will result in $\nabla_{INC} < 0$, since $V_k > V_{k-1}$. In this case the *INC* takes the *wrong decision* for the next perturbation.

Based on the above four cases, it can be concluded that the overall performance of *P&O* and *INC* in variable irradiance conditions are identical. The difference that has been introduced by the discrete implementation of the *INC* is such that it may favor the *INC* during increasing irradiance, while it may favor the *P&O* during decreasing irradiance.

F. Quantification of the discretization error's effect in dynamic conditions

In order to quantify the effect of the non-zero ∇_{INC}, in (25) the same reference irradiance ramp will be used again, for which, at an arbitrary point on the *IV* curve, the condition in (22) for the *P&O* is fulfilled. Equation (25) shows that the limit condition of INC is slightly different from the limit condition of *P&O*. To determine the boundary condition for *INC*, ∇_{INC} from (24) is set to zero, and the corresponding P_k^G is calculated.

$$\frac{I_k^G - I_{k-1}}{V_k - V_{k-1}} + \frac{I_k^G}{V_k} = 0 \tag{26}$$

After bringing the fractions to common denominator, then eliminating the denominator will result in:

$$I_k^G V_k - I_{k-1} V_k + I_k^G V_k - I_k^G V_{k-1} = 0 \tag{27}$$

Considering that $P_k^G = I_k^G V_k$, and $P_{k-1} = I_{k-1} V_{k-1}$, from the above follows:

$$P_k^G \left(2 - V_{k-1}/V_k\right) = P_{k-1} V_k / V_{k-1} \tag{28}$$

The above equation is suitable to show the relationship between P_k^G and P_{k-1} in function of V_k and V_{k-1}:

$$\frac{P_k^G}{P_{k-1}} = \frac{\left(V_k / V_{k-1}\right)^2}{2\left(V_k / V_{k-1}\right) - 1} \tag{29}$$

Fig. 6 displays the plot of P_k^G / P_{k-1} versus V_k / V_{k-1} and it shows that as long as $\Delta V \neq 0$ ($V_k / V_{k-1} \neq 1$), there is a difference between the points where the *P&O* and *INC* reach boundary conditions. It can also be seen that for *INC*, the limit condition is always met at $P_k^G / P_{k-1} > 1$, which causes a slight displacement of its tracking pattern compared to *P&O* (see Fig. 3).

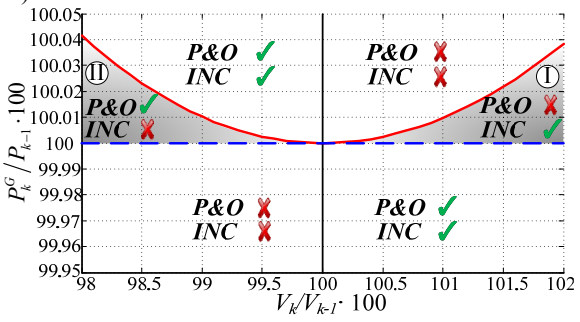

Fig. 6: Boundary conditions of correct (√) and wrong (*X*) tracking for *P&O (dashed line)* and *INC (continuous line)*, on the right-hand side of V_{mp}. In case the operating point voltage is smaller than V_{mp}, the correct/wrong tracking areas are reversed. Zones I and II denote the areas where *P&O* and *INC* behave differently.

In Fig. 6, at a voltage step of 1%, the boundary condition for *INC* is fulfilled when $P_k^G = 1.0001 \cdot P_{k-1}$.The condition in (22) for *P&O* is fulfilled when $P_k^G = P_{k-1}$, regardless of the perturbation size. This displacement theoretically favors *INC* during increasing irradiance (area I in Fig. 6) but disfavors it during decreasing irradiance (due to area II in Fig. 6).

However, in practice, the above displacement remains insignificant. PV inverters typically have a tracking speed ranging from 0.1% to 1% of V_{mp} in one second ($V_{mp}/10^3$/s –

$V_{mp}/10^2$/s) [42], but can be as fast as 2% of nominal V_{mp} per second [1].

Modern MPPTs have update frequencies of 10Hz or above [40], which correspond to voltage steps of ΔV<0.5% of nominal V_{mp} resulting in about 0.0025% difference between P_{k-1} and P_k^G in Fig. 6. This is an order below the basic power accuracy of the high precision power analyzer in [43], which is 0.02% of the reading value, and it is not realistic for a commercial PV inverter to match this power measurement accuracy, especially when measurement noise, ripple etc. are taken into account.

III. EXPERIMENTAL TESTS AND RESULTS

A. Test setup

The test setup consists of the following components: 1000V/40A high bandwidth PV simulator (Regatron TopCon Quadro with a linear post-processing unit TC.LIN), a custom-built 800W DC/DC boost converter connected to a 2.2kW Danfoss VLT-FC302 inverter, which is then connected to the grid through an LC filter and a 1:1 transformer (Fig. 7). The PV simulator emulates a preloaded I-V curve of the PV array as given in II.A, corresponding to the EN 50530 standard's requirements for the PV simulator specifications.

The control structure has been implemented in Simulink, and using the dSPACE Real-Time Interface, it has been compiled and downloaded to the dSpace 1103 controller board. The control structure for the grid connected converter is a classical one based on resonant controller. The DC/DC boost converter unit has its own voltage and current sensing (V_{pv} and I_{pv}), as well as the voltage control implemented on a Texas Instruments TMS320F335 controller board.

The MPPT unit, implemented in the dSpace controller, receives V_{pv} and I_{pv}, and sends the reference, V_{pv} *ref,* back to the converter through CAN bus.

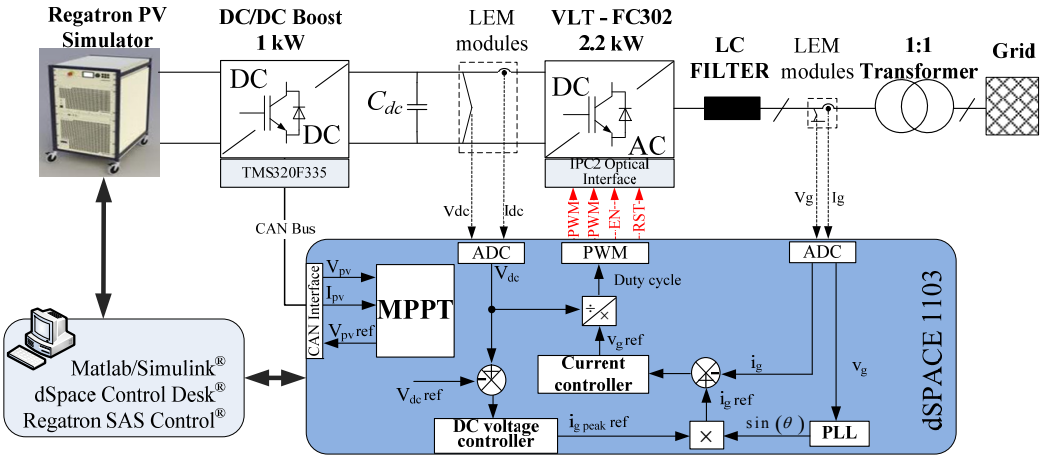

Fig. 7: Simplified diagram of the experimental setup, including the main control structure

B. Test conditions

The considered PV array is crystalline Si with P_{mp} = 700W and V_{mp} = 300V in STC[1]. The DC link voltage (V_{dc} in Fig. 7) was kept constant at 450V by the inverter's DC link voltage controller.

The MPPT methods have been implemented with the following sets of identical perturbation frequencies (f_{MPPT}) and perturbation amplitudes (ΔV): 1: $f_{MPPT} = 10Hz$, $\Delta V = 1V$; 2: $f_{MPPT} = 10Hz$, $\Delta V = 2V$, and 3: $f_{MPPT} = 5Hz$, $\Delta V = 1V$. These values have been chosen according to common MPPT voltage adjustment speeds [42].

All tests have been carried out according to the EN 50530 standard: "Overall efficiency of grid connected photovoltaic inverters" [32]. In the following, a brief description of the EN 50530 requirements is given.

1) EN 50530 requirements in static conditions

EN 50530 requires the measurement of static MPPT efficiency at a series of well-defined power levels according to the European Efficiency (η_{EUR}) and Californian Efficiency (η_{CEC}). The formulae for the η_{EUR} and η_{CEC} are given below:

$$\eta_{EUR} = 0.03\cdot\eta_{5\%} + 0.06\cdot\eta_{10\%} + 0.13\cdot\eta_{20\%} + 0.1\cdot\eta_{30\%} + 0.48\cdot\eta_{50\%} + 0.2\cdot\eta_{100\%} \quad (30)$$

$$\eta_{CEC} = 0.04\cdot\eta_{10\%} + 0.05\cdot\eta_{20\%} + 0.12\cdot\eta_{30\%} + 0.21\cdot\eta_{50\%} + 0.53\cdot\eta_{75\%} + 0.05\cdot\eta_{100\%} \quad (31)$$

The indices of 5%, 10% etc. in the above equations refer to power levels of corresponding fractions of STC, i.e. $\eta_{5\%}$refers to MPPT efficiency at 5% of STC (rated) power, and so on. The corresponding static efficiencies are calculated as:

$$\eta_{stat,k} = \frac{\sum_k P_{PV,meas}\cdot\Delta T}{P_{mp}\cdot T_M} \quad (32)$$

In (32), P_{mp} is provided by the PV simulator, ΔT is the sampling period, k refers to the actual power level, e.g. 5%, 10%, etc., and T_M is the total measurement period for the given power level (10 min).

The η_{EUR} and η_{CEC} must be calculated at three different voltage levels, corresponding to the rated (V_{mp} *rtd*), minimum (V_{mp} *min*) and maximum (V_{mp} *max*) MPP voltages of the PV inverter.

2) EN 50530 requirements in dynamic conditions

In order to evaluate their dynamic performance, the MPP trackers are subjected to variable irradiance conditions, in a trapezoidal shape, from 10 to 50% of STC irradiance, as

[1] Standard Test Conditions - test conditions to measure PV cells/modules nominal output power. Irradiance is 1000W/m^2, solar spectral distribution corresponds to air mass 1.5 and cell/module junction temperature is 25°C.

shown in Fig. 8. The times t1, t2, t3 and t4 determine the speed of irradiance change, and N defines the number of repetition for each profile, which forms a sequence. EN 50530 requires the use of 11 sequences, with well-defined t1, t2, t3, t4, and N, with increasing steepness of the trapezoidal irradiance profiles.

In the next step a second series of sequences, similar to the above described, are applied, from 30% to 100% of STC irradiance.

Finally, the dynamic MPPT efficiency is calculated as:

$$\eta_{dyn} = \frac{1}{K}\sum_{i=1}^{K}\eta_{dyn,i}, \quad where \quad \eta_{dyn,i} = \frac{\sum_i P_{PV,meas}\cdot\Delta T}{\sum_i P_{mp}\cdot\Delta T} \qquad (32)$$

In the above equations, ΔT is the sampling period, and P_{mp} is provided by the PV simulator.

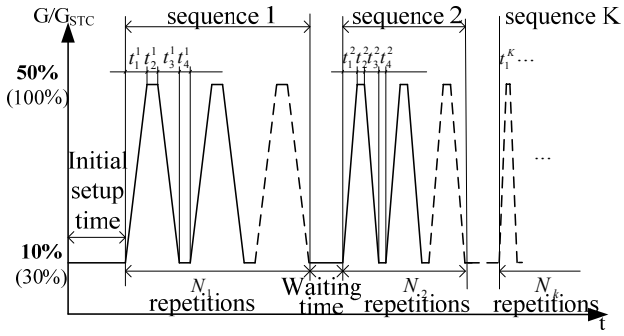

Fig. 8: Trapezoidal irradiance profiles for testing the dynamic performance of MPPTs, according to EN 50530.

C. Experimental results

1) Static conditions

Table 1 below summarizes the measured EN 50530 EUR and CEC efficiencies for *P&O* and *INC*, calculated with a resolution of two decimals. MPPT efficiencies for PV inverters are normally given with one [40] or no decimals [1].

Table 1: Experimental results: η_{EUR} and η_{CEC}

$f_{MPPT}/\Delta V$		*P&O*	*INC*	|*P&O-INC*|
10Hz/1V	η_{EUR} at V_{mp} *min*	99.80 %	99.80 %	0.00 %
	η_{CEC} at V_{mp} *min*	99.85 %	99.85 %	0.00 %
	η_{EUR} at V_{mp} *rtd*	99.77 %	**99.78 %**	0.01 %
	η_{CEC} at V_{mp} *rtd*	99.83 %	99.83 %	0.00 %
	η_{EUR} at V_{mp} *max*	99.59 %	**99.61 %**	0.02 %
	η_{CEC} at V_{mp} *max*	**99.82 %**	99.81 %	0.01 %
	η_{EUR} *average*	*99.72 %*	*99.73 %*	*0.01 %*
	η_{CEC} *average*	*99.83 %*	*99.83 %*	*0.00 %*
10Hz/2V	η_{EUR} at V_{mp} *min*	99.79%	99.79%	0.00%
	η_{CEC} at V_{mp} *min*	99.83%	99.83%	0.00%
	η_{EUR} at V_{mp} *rtd*	99.74%	99.74%	0.00%
	η_{CEC} at V_{mp} *rtd*	**99.81%**	99.80%	0.01%
	η_{EUR} at V_{mp} *max*	99.72%	99.72%	0.00%
	η_{CEC} at V_{mp} *max*	99.79%	99.79%	0.00%
	η_{EUR} *average*	*99.75%*	*99.75%*	*0.00%*
	η_{CEC} *average*	*99.81%*	*99.81%*	*0.00%*

V_{mp} *min* = 250V, V_{mp} *rtd* = 300V, V_{mp} *max* = 350V

It can be seen from the above that *P&O* and *INC* perform extremely close, in most cases showing the same efficiencies, with a maximum deviation of 0.02%, which is well within the statistical variations between successive tests of the same tracker. In static conditions only two different ΔV –s have been considered, as it is not expected that f_{MPPT} to have a significant effect on the tracking performance, as long as it does not approach the converter's bandwidth [4].

2) Dynamic conditions

In order to verify the repeatability of the results, similarly to the cases of static EUR and CEC efficiencies where the same tests were carried out at three different voltage levels, the EN 50530 dynamic tests have been also repeated three times. The results are summarized in Table 2, below:

Table 2: Experimental results: dynamic efficiencies

$f_{MPPT}/\Delta V$		*P&O*	*INC*	|*P&O-INC*|
10Hz/1V	η_{dyn} test 1	**98.26 %**	97.51 %	0.75 %
	η_{dyn} test 2	97.78 %	**98.17 %**	0.39 %
	η_{dyn} test 3	**97.72 %**	97.69 %	0.03 %
	η_{dyn} avg.	*97.92 %*	*97.79 %*	*0.13 %*
5Hz/1V	η_{dyn} test 1	**95.64%**	95.62%	0.02%
	η_{dyn} test 2	**95.38%**	94.90%	0.48%
	η_{dyn} test 3	95.45%	**95.61%**	0.16%
	η_{dyn} avg.	*95.49%*	*95.38%*	*0.11%*
10Hz/2V	η_{dyn} test 1	**98.86%**	98.77%	0.09%
	η_{dyn} test 2	98.67%	**98.80%**	0.13%
	η_{dyn} test 3	98.82%	**98.83%**	0.01%
	η_{dyn} avg.	*98.78%*	*98.80%*	*0.02%*

As can be seen in Table 2, the dynamic performances are again very close. Their efficiencies, averaged over the three test runs, show a deviation well below the statistical variations between successive tests of the same tracker, for all f_{MPPT}.and ΔV combinations. These results are in good agreement with the outdoor results reported in [31].

IV. CONCLUSIONS

The results of the analysis show that the tracking performances of *P&O* and *INC* are largely identical in both static and dynamic conditions.

They are both based on the same mathematical relation of the derivative of power with voltage, and it has been shown that the only difference between them is that the *INC* neglects the second order term in the discrete differentiation of the power. Detailed experimental tests have been carried out according to the EN 50530 standard and the resulting efficiency deviations in static conditions are below 0.02% in η_{EUR} and below 0.01 in η_{CEC}. In dynamic conditions, this deviation is below 0.15%. In both static and dynamic conditions, the differences between the two trackers are within the statistical variations among successive tests of the same method.

Considering that they share the same principle, show equal behavior and equal performance, it can be concluded that the two methods are equivalent.

It is hoped that this analysis will be useful for researchers and industry alike when selecting a suitable hill-climbing MPPT for their application.

Finally, the recommendation of the authors is that *INC* is not treated as a separate MPPT, but a specific implementation of the *P&O* algorithm.

V. REFERENCES

[1] PHOTON International, "An all-round success," *PHOTON International*, pp. 159–169, Jun-2010.

[2] N. Femia, G. Petrone, G. Spagnuolo, and M. Vitelli, *Power Electronics and Control Techniques for Maximum Energy Harvesting in Photovoltaic Systems*. Boca Raton, FL: CRC PressISBN:978-1-4665-0690-9, 2013.

[3] L. Egiziano, N. Femia, D. Granozio, G. Petrone, G. Spagnuolo, and M. Vitelli, "Photovoltaic inverters with Perturb & Observe MPPT technique and one-cycle control," *Proc of IEEE ISCAS*, 2006.

[4] N. Femia, G. Petrone, G. Spagnuolo, and M. Vitelli, "Optimization of Perturb and Observe maximum power point tracking method," *IEEE T. Power. Electr.*, vol. 20, no. 4, pp. 963–973, 2005.

[5] X. Liu and L. A. C. Lopes, "An improved perturbation and observation maximum power point tracking algorithm for PV arrays," *Proc. of IEEE PESC*, pp. 2005–2010, 2004.

[6] N. Femia, G. Petrone, G. Spagnuolo, and M. Vitelli, "Optimizing duty-cycle perturbation of P&O MPPT technique," *Proc of IEEE PESC*, 2004, vol. 3, no. 1, pp. 1939–1944.

[7] K.-H. Chao and C.-J. Li, "An intelligent maximum power point tracking method based on extension theory for PV systems," *Expert Syst. Appl.*, vol. 37, no. 2, pp. 1050–1055, Mar. 2010.

[8] F. Zhang, K. Thanapalan, J. Maddy, and A. Guwy, "Development of a novel hybrid maximum power point tracking methodology for photovoltaic systems," *Proc of IEEE ICAC*, 2012, no. September.

[9] N. Kasa, T. Iida, and G. Majumdar, "Robust control for maximum power point tracking in photovoltaic power system," *Proc of IEEE PCC*, 2002, vol. 2, pp. 827–832.

[10] D. P. Hohm and M. E. Ropp, "Comparative study of maximum power point tracking algorithms using an experimental, programmable, maximum power point tracking test," *Proc of IEEE PVSC*, 2000, pp. 1699–1702.

[11] K. Tse, M. Ho, H. S. H. Chung, and S. Hui, "A novel maximum power point tracker for PV panels using switching frequency modulation," *IEEE T. Power. Electr.*, vol. 17, no. 6, 2002.

[12] W. Wu, N. Pongratananukul, W. Qiu, K. Rustom, T. Kasparis, and I. Batarseh, "DSP-based multiple peak power tracking for expandable power system," *Proc of IEEE APEC*, 2003, vol. 1, no. C, pp. 525–530.

[13] T. Esram and P. L. Chapman, "Comparison of Photovoltaic Array Maximum Power Point Tracking Techniques," *IEEE T. Energy. Conver.*, vol. 22, no. 2, pp. 439–449, 2007.

[14] V. Salas, E. Olías, A. Barrado, and A. Lázaro, "Review of the maximum power point tracking algorithms for stand-alone photovoltaic systems," *Sol. Energy Mater. Sol. Cells*, vol. 90, no. 11, pp. 1555–1578, Jul. 2006.

[15] N. Femia, D. Granozio, G. Petrone, G. Spagnuolo, M. Vitelli, I. Introduction, and A. S. I. Conditions, "Predictive & Adaptive MPPT Perturb and Observe Method," *IEEE T. Aero. Elec. Sys.*, vol. 43, no. 3, pp. 934–950, 2007.

[16] N. Femia, G. Petrone, G. Spagnuolo, and M. Vitelli, "Perturb and Observe MPPT technique robustness improved," *Proc of IEEE PESC*, 2004, vol. 3, no. 1, pp. 845–850 o. 2.

[17] C. W. Tan, T. C. Green, and C. A. Hernandez-Aramburo, "An improved maximum power point tracking algorithm with current-mode control for photovoltaic applications," *Proc of IEEE PEDS*, 2005, vol. 1, no. 2, pp. 489–494.

[18] D. Sera, R. Teodorescu, J. Hantschel, and M. Knoll, "Optimized maximum power point tracker for fast changing environmental conditions," *IEEE T. Ind. Electron.*, vol. 55, no. 7, 2008.

[19] I. S. Kim, M. B. Kim, and M. J. Youn, "New maximum power point tracker using sliding-mode observer for estimation of solar array current in the grid-connected photovoltaic system," *IEEE T. Ind. Electron.*, vol. 53, no. 4, pp. 1027–1035, 2006.

[20] J.-M. Kwon, K.-H. Nam, and B.-H. Kwon, "Photovoltaic power conditioning system with line connection," *IEEE T. Ind. Electron.*, vol. 53, no. 4, pp. 1048–1054, 2006.

[21] F. A. Inthamoussou, H. De Battista, and R. J. Mantz, "New concept in maximum power tracking for the control of a photovoltaic/hydrogen system," *Int. J. Hydrogen Energy*, vol. 37, no. 19, pp. 14951–14958, Oct. 2012.

[22] C. Hua and C. Shen, "Comparative study of peak power tracking techniques for solar storage system," *Proc of IEEE APEC*, 1998, vol. 2, no. 1, pp. 679–685.

[23] T. Y. Kim, H. G. Ahn, S. K. Park, and Y. K. Lee, "A novel maximum power point tracking control for photovoltaic power system under rapidly changing solar radiation," *Proc of IEEE ISIE*, 2001, vol. 2, pp. 1011–1014.

[24] C. T. Pan, J. Y. Chen, C. P. Chu, and Y. S. Huang, "A fast maximum power point tracker for photovoltaic power systems," *Proc of IEEE IECON*, 1999, vol. 1, pp. 390–393.

[25] C. Hua, J. Lin, and C. Shen, "Implementation of a DSP-controlled photovoltaic system with peak power tracking," *IEEE T. Ind. Electron.*, vol. 45, no. 1, pp. 99–107, 1998.

[26] G. J. Yu, Y. S. Jung, J. Y. Choi, and G. S. Kim, "A novel two-mode MPPT control algorithm based on comparative study of existing algorithms," *Solar Energy*, vol. 76, no. 4, pp. 455–463, Apr. 2004.

[27] A. Zegaoui, M. Aillerie, P. Petit, J. P. Sawicki, A. Jaafar, C. Salame, and J. P. Charles, "Comparison of Two Common Maximum Power Point Trackers by Simulating of PV Generators," *Energy Procedia*, vol. 6, pp. 678–687, Jan. 2011.

[28] T. Tafticht, K. Agbossou, and M. L. Doumbia, "A new MPPT method for photovoltaic systems used for hydrogen production," *COMPEL*, vol. 26, no. 1, pp. 62–74, 2007.

[29] H. Koizumi, "A novel maximum power point tracking method for PV module integrated converter using square root functions," *Proc of IEEE IECON*, 2005.

[30] B. M. Wilamowski and X. Li, "Fuzzy system based maximum power point tracking for PV system," *Proc of IEEE IECON*, 2002, vol. 4, no. I, pp. 3280–3284.

[31] S. B. Kjaer, "Evaluation of the 'Hill Climbing'and the 'Incremental Conductance' Maximum Power Point Trackers for Photovoltaic Power Systems," *IEEE T. Energy. Conver.*, vol. 27, no. 4, pp. 922–929, 2012.

[32] European Committee of Electrotechnical Standardization, *European Standard EN 50530 - Overall efficiency of grid connected photovoltaic inverters*. 2010.

[33] J. A. Gow and C. D. Manning, "Development of a photovoltaic array model for use in power-electronics simulation studies," *IET Electr. Power Appl.*, vol. 146, no. 2, pp. 193–200, 1999.

[34] H. Haeberlin and L. Borgna, "A new approach for semi-automated measurement of PV inverters, especially MPP tracking efficiency, using a linear PV array simulator with high stability," *Proc of EUPVSEC*, 2004, no. June, pp. 7–11.

[35] G. Petrone, G. Spagnuolo, and M. Vitelli, "Analytical model of mismatched photovoltaic fields by means of Lambert W-function," *Sol. Energy Mater. Sol. Cells*, vol. 91, no. 18, pp. 1652–1657, Nov. 2007.

[36] D. Sera, R. Teodorescu, and P. Rodriguez, "PV panel model based on datasheet values," *Proc of IEEE ISIE*, 2007, no. 4.

[37] K. H. Hussein, I. Muta, T. Hoshino, and M. Osakada, "Maximum photovoltaic power tracking: an algorithm for rapidly changing atmospheric conditions," *IEE Proc. Gen., Transm. & Distr.*, vol. 142, no. 1, pp. 59–64, 1995.

[38] O. Wasynezuk, "Dynamic behavior of a class of photovoltaic power systems," *IEEE T. Power. Ap. Syst.*, vol. PAS-102, no. 9, 1983.

[39] K. Lee, Y. Fujii, T. Sumiya, and E. Ikawa, "Development of a 250kW PV PCS and Adaptive MPPT Method," *Proc of Int Pow Electr Conf*, 2010, pp. 2598–2602.

[40] Danfoss Solar Inverters, "Supreme Maximum Power Point Tracking efficiency," 2011. [Online]. Available: http://www.danfoss.com/NewsAndEvents/Archive/Solar+Energy+News/Supreme-Maximum-Power-Point-Tracking-efficiency/62E02010-F50C-4AE3-845D-7A5B73F6F6AE.html. [Accessed: 29-Oct-2012].

[41] D. Sera, T. Kerekes, R. Teodorescu, and F. Blaabjerg, "Improved MPPT algorithms for rapidly changing environmental conditions," *Proc of EPE-PEMC*, 2006, pp. 1420–1425.

[42] H. Schmidt, B. Burger, U. Bussemas, and S. Elies, "How fast does an MPP tracker really need to be?," *Proc of EUPVSEC*, 2009, no. September, pp. 3273–3276.

[43] Yokogawa Electric Corporation, "WT3000 Precision Power Analyzer User's Manual," 2008.

Dezso Sera (S'05-M'08) received his B.Sc. and M.Sc. degrees in Electrical Engineering from the Technical University of Cluj, Romania in 2001 and 2002, respectively.
In 2005, he graduated from the M.Sc. program at Aalborg University, Denmark, in the Department of Energy Technology (DET) and in 2008 he received his PhD degree from the same department, where he currently works as Associate Professor. Since 2009 he has been the coordinator of the Photovoltaic Systems Research Programme at DET. His current research activities are in photovoltaic power systems, specifically in the modelling, characterisation, diagnostics and maximum power point tracking (MPPT) of PV systems, grid integration of PV power, power electronics.

Laszlo Mathe (S'07–M'10) received the B.Sc. degree in electrical engineering and the M.Sc. degree from the Technical University of Cluj-Napoca, Cluj-Napoca, Romania, in 2000 and 2002, respectively. Between 2002 and 2007 he was working as a Control Development Engineer. In 2007 he was enrolled in as a PhD fellow at the Department of Energy Technology, Aalborg University, Denmark, and in 2010 he received his Ph.D. degree in electrical engineering. He is currently an Assistant Professor with Aalborg University. His current research activities are in PV systems, modulation techniques (MMC, two level inverters), motor control, electric vehicle, SiC based inverter design.

Tamas Kerekes (S'05-M'10) obtained his Electrical Engineer diploma in 2002 from Technical University of Cluj, Romania, with specialization in Electric Drives and Robots. In 2005, he graduated the Master of Science program at Aalborg University, Department of Energy Technology in the field of Power Electronics and Drives. In 2009 he received his PhD degree from Aalborg University. Currently he is working as an Associate Professor at the same Department. Since he started his PhD at the Department of Energy Technology his main interest is on PV inverter modelling, control and topologies as well as modulation techniques with focus on transformerless PV inverter systems.

Sergiu Viorel Spataru (S'10) was born in Arad, Romania, in 1985.He received his B.Sc. degree in electrical engineering, in 2009, from the "Politehnica" University of Timisoara (UPT), Romania. In 2011 he received his M.Sc. degree in wind power systems from Aalborg University (AAU), Denmark, where he is currently working towards his Ph.D. degree.
His current research interests include characterization methods for photovoltaic modules, data analysis, modelling and machine learning methods applied to diagnostic and condition monitoring of photovoltaic power systems

Remus Teodorescu (S'96–A'97–M'99–SM'02-F'12) received the Dipl. Ing. degree in electrical engineering from Polytechnic University of Bucharest, Romania in 1989, and PhD degree in power electronics from University of Galati, Romania, in 1994. In 1998, he joined Aalborg University, Department of Energy Technology, power electronics section where he currently works as a professor. He has more than 200 papers published, 1 book ("Grid Converters for Photovoltaic and Wind Power Systems", ISBN-10: 0-470-05751-3 – Wiley) and 5 patents. He is an IEEE Fellow, Past Associate Editor for IEEE Transactions on Power Electronics Letters and chair of IEEE Danish joint IES/PELS/IAS chapter. He is the founder and coordinator of the Green Power Laboratory at Aalborg University focusing on the development and testing of grid converters for renewable energy systems. He is the coordinator of Vestas Power Program, involving 10 PhD students and guest professors in the areas of power electronics, power systems and energy storage. His areas of interests are: design and control of power converters used in photovoltaics and wind power systems, grid integration with wind power, medium-voltage converters, HVDC/FACTS, energy storage.